Hindawi
Journal of Nanomaterials
Volume 2019, Article ID 2784708, 9 pages
https://doi.org/10.1155/2019/2784708

Research Article

Facile Synthesis of a Tailored-Designed Au/Pt Nanoanode for Enhanced Formic Acid, Methanol, and Ethylene Glycol Electrooxidation

Islam M. Al-Akraa,[1] **Yaser M. Asal**,[1] **and Ahmad M. Mohammad**[2]

[1]*Department of Chemical Engineering, Faculty of Engineering, The British University in Egypt, Cairo 11837, Egypt*
[2]*Chemistry Department, Faculty of Science, Cairo University, Cairo 12613, Egypt*

Correspondence should be addressed to Islam M. Al-Akraa; islam.ahmed@bue.edu.eg
and Ahmad M. Mohammad; ammohammad@cu.edu.eg

Received 29 August 2018; Revised 15 October 2018; Accepted 4 November 2018; Published 3 January 2019

Academic Editor: Hassan Karimi-Maleh

The recent revolution in nanoscience and global energy demand have motivated research in liquid fuel cells (LFCs) due to their enhanced efficiency, moving flexibility, and reduced contamination. In line with this advancement, a glassy carbon (GC) electrode was modified with platinum (PtNPs) and gold (AuNPs) nanoparticles to fabricate a nanosized anode for formic acid, methanol, and ethylene glycol electrooxidation (abbreviated, respectively, to FAO, MO, and EGO), of the key anodic reactions of LFCs. The deposition sequence of the catalyst's layers was important where the Au/Pt/GC electrode (in which PtNPs were directly deposited onto the GC surface followed by AuNPs—surface coverage ≈ 32%) exhibited the best catalytic performance. The catalytic performance of the Au/Pt/GC anode excelled (at least threefold) its value obtained at the Pt/GC anode with regard to FAO and EGO, if the oxidation peak currents were compared. This enhancement got reduced to 1.4 times in the case of MO, but the large decrease (− 220 mV) in the onset potential of MO provided compensation. The role of AuNPs in the Au/Pt/GC catalyst was principal in boosting its catalytic performance as it immunized the underlying PtNPs against CO poisoning which is associated with the release of CO as an intermediate during the oxidation. Interestingly, AuNPs succeeded in interrupting the contiguity of the Pt surface sites required for CO adsorption during FAO, MO, and EGO and, thus, presage preventing the deterioration of the catalytic performance of their corresponding LFCs.

1. Introduction

The world is adopting right now legislations to avoid the depletion of natural resources in a way that maintains sustainability [1]. Sustainable resources, accordingly, should neither get significantly depleted over time nor result in serious health or environmental hazards [2, 3]. In this regard, fossil fuels which for a long time represented the major resource for power production and consumption were exempted from being sustainable. Besides being rapidly depleted, fossil fuels in the traditional combustion schemes contaminate the environment with substantial carbon emissions. That necessitated switching to renewable power schemes with regard to production, transmission, and storage to fulfill desired life prosperity. Of the best (greenest) methodologies to save power in renewable plants is the use of water-based electrolyzers to convert excessive energy into H_2 and O_2 that, when needed, are purged into typical H_2/O_2 fuel cells (HFCs) to produce electricity back for useful applications [3, 4]. That activated the market of fuel cells (FCs) which is now already concerned with the production of portable power systems such as the electric vehicle and multiple stationary electrical and backup systems [5]. In fact, FCs with their enhanced efficiency (up to 60% in electrical energy conversion and up to 80% of electricity and heat), greenness (more than 90% reduction in major pollutants emerged with fossil fuel combustion) reliability, robustness, safety, and moving flexibility represent a paradigm in the

judicious development of clean and efficient power generation systems [5, 6]. The key function of FCs is a galvanic conversion of chemical energy released from the combustion of a fuel into electricity. The selection of a fuel passes through a number of criteria including its availability, cost, toxicity, calorific value, storage, density, phase, water content, purity, security of supply, and carbon content. Hydrogen, the lightest carbon-free fuel, has been the focus of fundamental and applied research for potential applications in HFCs. However, the high cost of miniaturized hydrogen containers; the potential risk associated with using, storing, and transporting hydrogen; and its low gas-phase energy density have driven the attention towards liquid fuels such as formic acid (FA) [7], methanol (M) [8], and ethylene glycol (EG) [9]. Interestingly, the FCs of these particular fuels have shown inherent features that excel from those of HFCs. For example, the direct formic acid FCs (DFAFCs) enabled the direct use of liquid fuels without a reformer (a reactor for H_2 production) and offered the potential for enhanced cell performance by lowering the fuel crossover [10]. Alternatively, the direct methanol FCs (DMFCs) represented a reasonable convenience employing a small liquid fuel and offering a high a theoretical energy density (4690 Wh L^{-1}) [11]. On the other hand, the direct ethylene glycol FCs (DEGFCs) utilized the impressive hydrogen content and high boiling point of EG and possessed a high volumetric energy density (5900 Wh L^{-1}) [9]. However, it remained essential to optimize the electrooxidation of these fuels (denoted, respectively, FAO, MO, and EGO) to limit the significant overpotential loss and any possible poisoning associating the operation of their corresponding FCs. A major drawback which deteriorates the performance of these liquid FCs is the poisoning of the typical Pt-based anodes with intermediates (e.g., CO) released during FAO, MO, and EGO [12]. Recently, we can minimize this poisoning for FAO by modifying the Pt surface with gold nanoparticles (AuNPs) in a way which distorts the contiguity of the active Pt sites required for CO adsorption (what is known as ensemble or third-body effect) [13]. Herein, the investigation is expanded to evaluate the impact of this modification for MO and EGO as well. Promisingly, by loading AuNPs at the Pt surface, the catalytic activity of FAO, MO, and EGO could largely be enhanced, with a concurrent significant mitigation of CO poisoning.

2. Materials and Methods

2.1. Electrodes. Glassy carbon (GC, $d = 5.0$ mm) electrode was served as a working electrode after cleaning with a conventional cleaning procedure. Typically, the electrode was mechanically polished with no. 2000 emery paper, then with aqueous slurries of successively finer alumina powder (down to 0.06 μm) with the help of a polishing microcloth. Next, the polished electrode was rinsed thoroughly with distilled water. A saturated calomel electrode (SCE) and a spiral Pt wire were used as reference and counter electrodes, respectively. All potentials in this investigation were measured in reference to SCE.

2.2. Electrodeposition of PtNPs and AuNPs. All the chemicals used in this investigation were of analytical grade and used without prior purification. The electrodeposition of PtNPs was carried out in 0.1 M Na_2SO_4 containing 2.0 mM H_2PtCl_6 solution by holding the potential at 0.1 for 300 s according to the following electrochemical equation:

$$Pt^{4+} + 4e^- \longrightarrow Pt \quad (1)$$

Alternatively, the electrode's modification with AuNPs was carried out in 0.1 M Na_2SO_4 containing 1.0 mM $KAuCl_4$ solution by holding the potential at 0.1 V for 300 s according to the following equation:

$$Au^{3+} + 3e^- \longrightarrow Au \quad (2)$$

2.3. Electrochemical and Material Characterization. The electrochemical measurements were performed at room temperature ($25 \pm 1^\circ$C) in a two-compartment three-electrode glass cell. The measurements were performed using a Bio-Logic SAS potentiostat (model SP-150) operated with EC-Lab software. Current densities were calculated on the basis of the real surface area of the working electrodes. The electrocatalytic activity of the modified electrodes toward FAO, MO, and EGO was examined in an aqueous solution (0.3 M) of the corresponding fuel at a scan rate of 100 mV s^{-1}.

The current investigation will principally compare the electrochemical characterization and activity toward FAO, MO, and EGO for two electrodes: PtNPs' modified GC (abbreviated as Pt/GC) and AuNPs' modified Pt/GC (abbreviated as Au/Pt/GC) electrodes.

A field emission scanning electron microscope (FE-SEM, QUANTA FEG 250), coupled with an energy-dispersive X-ray spectrometer (EDS), was employed to disclose the electrode's morphology and composition. The crystallographic structure of the modified catalysts was revealed using X-ray diffraction (XRD, PANalytical, X'Pert PRO) operated with a Cu target ($\lambda = 1.54$ Å).

3. Results and Discussion

3.1. Electrochemical and Material Characterization. The electrochemical characterization techniques are very powerful and sensitive to very low concentrations even to traces from active ingredients and can moreover, in certain circumstances, distinguish firmly between the different types of surface atoms as in our case of Pt and Au. Figure 1 shows the typical Pt and Au characteristic CVs obtained on Pt/GC-, Au/GC-, and Au/Pt/GC-modified electrodes in acidic conditions. In Figure 1, a, the characteristic behavior of a polycrystalline Pt electrode is clearly shown; the oxidation of Pt, which extends over a wide range of potentials (0.6 to 1.5 V), is coupled with the reduction peak at ca. 0.25 V. This couple corresponds to the solid-state surface redox transition (SSSRT) involving PtO/Pt. In addition, well-defined peaks for the hydrogen adsorption/desorption ($H_{ads/des}$) are shown in the potential range from 0.0 to −0.35 V [14]. On the other hand, in Figure 1, b, the gold oxide

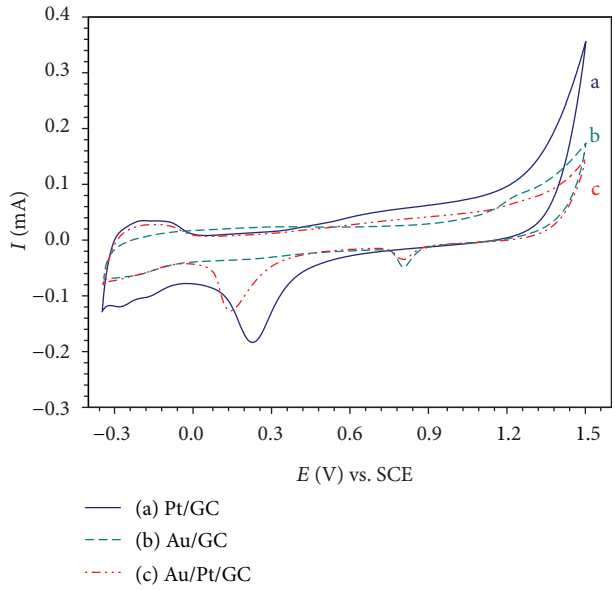

FIGURE 1: CVs obtained on (a) Pt/GC, (b) Au/GC, and (c) Au/Pt/GC electrodes in 0.5 M H_2SO_4. Potential scan rate: 100 mV s^{-1}.

formation started at ca. 1.1 V and the oxide reduction peak appeared at ca. 0.85 V.

When AuNPs were deposited on the Pt/GC electrode (Figure 1, c), a decorated nanoparticle structure was obtained where the exposed surface area of Pt, in the case of the Pt/GC electrode, decreased by 32%. In other words, the surface coverage of AuNPs, θ, can be estimated (compare Figures 1, c, and 1, a).

$$\theta = \left(1 - \frac{A_{r(Au/Pt/GC)}}{A_{r(Pt/GC)}}\right) \times 100 \approx 32\%. \quad (3)$$

Moreover, the PtO reduction peak was shifted to a more cathodic potential which inferred a change in the surface composition of the catalyst [15].

Morphologically, Figure 2 shows the FE-SEM images of the Pt/GC (panel a) and Au/Pt/GC (panel b) electrodes. It depicted the deposition of well-dispersed spherical Pt particles with an average particle size of ca. 60 nm onto the GC electrode (Figure 2(a)). The modification of the Pt/GC electrode with AuNPs (Au/Pt/GC electrode, Figure 2(b)) resulted in a decorated nanowire structure (average diameter = 50 nm) that homogeneously covered the entire surface of the GC electrode.

The EDS analysis of the Pt/GC (panel a) and Au/Pt/GC (panel b) electrodes confirmed the deposition of the different ingredients in the catalyst (PtNPs and AuNPs) and assisted in calculating their relative compositions (see Figure 3).

Additionally, the XRD analysis confirmed the deposition of PtNPs in the Pt/GC (Figure 4, a) and Au/Pt/GC (Figure 4, b) electrodes in a face-centered cubic (fcc) structure, where all the typical characteristic peaks of Pt (1 1 1), (2 0 0), (2 2 0), and (3 1 1) appeared at 2θ of 40°, 43°, 67°, and 78°, respectively [14]. As can be seen, no diffraction peaks have been observed for Au which might result from alloying AuNPs in the Pt lattice. The slight shift in 2θ of the diffraction peaks of Pt in the Au/Pt/GC electrode (Figure 4, b) might support this assumption. The diffraction peaks appeared at 2θ of 25° and 52° were assigned to the (0 0 2) and (1 0 0) crystallographic facets of the carbon support [16].

3.2. Electrocatalytic Activity and Stability toward FAO. Figure 5 shows the CVs of the FAO on the Pt/GC (Figure 5, a) and Au/Pt/GC (Figure 5, b) electrodes in 0.1 M NaOH solution containing 0.3 M FA (pH = 3.5). Commonly, on Pt-based catalysts, the FAO takes place through two parallel pathways [17]. The first (direct) includes the dehydrogenation of FA to CO_2. This is actually the favorable route for FAO as it happens at a low potential domain (low overvoltage), which eventually makes the actual cell voltage close to the theoretical value. Equation 4 represents the reaction of this pathway while the peak observed at ca. 0.4 V in the forward scan of Figure 5, a, at the Pt/GC electrode corresponds to FAO through this direct pathway.

$$HCOOH \longrightarrow CO_2 + 2H^+ + 2e^- \quad (4)$$

The peak current of this direct peak, $I_p{}^d$, is essential to assess the density of active (not poisoned) Pt sites that participated in the direct FAO. The other (indirect dehydration) pathway of FAO is unfavorable as it involves the oxidation of poisoning CO that is adsorbed on Pt surfaces even at the open circuit potential, and the other peak at 0.75 V ($I_p{}^{ind}$) in the forward scan of Figure 5, a, is assigned to this indirect oxidation reaction. At high potential, the CO_{ads} is oxidized by Pt-OH species that is formed at ca. 0.5 V during the forward scan, which activated back most of the Pt sites for FAO. In the backward scan (cathodic scan), while most of the CO_{ads} has been oxidatively desorbed at high potential, the FAO can then proceed on a clean Pt surface through the dehydrogenation pathway. This can be observed from the high current of the backward scan peak (I_b). Equations 5-7 describe the mechanism of the indirect pathway of FAO.

$$HCOOH + Pt \longrightarrow Pt - CO_{ads} + H_2O \quad (5)$$

$$H_2O + Pt \longrightarrow Pt - OH + H^+ + e^- \quad (6)$$

$$Pt - CO_{ads} + Pt - OH \longrightarrow 2Pt + CO_2 + H^+ + e^- \quad (7)$$

Three parameters will next be utilized to quantify the degree of catalytic enhancement toward FAO; one is the $I_p{}^d/I_p{}^{ind}$, the second is the $I_p{}^d/I_b$, and the third is the onset potential of FAO (E_{onset}). A high value of $I_p{}^d/I_p{}^{ind}$ indicates the availability of excess active Pt sites free to participate in the direct FAO at low potential, which actually results in saving energy. Alternatively, a high value of $I_p{}^d/I_b$ corresponds to a low value of CO poisoning level. Furthermore, a small (more negative) E_{onset} value correlates to less required overpotential that indicates a corresponding (thermodynamics) enhancement of FAO. At the Pt/GC

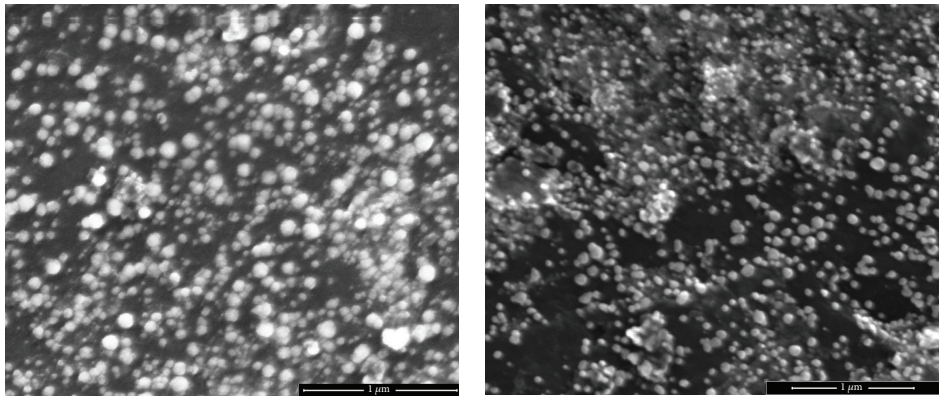

(a) (b)

Figure 2: FE-SEM images of (a) Pt/GC and (b) Au/Pt/GC electrodes.

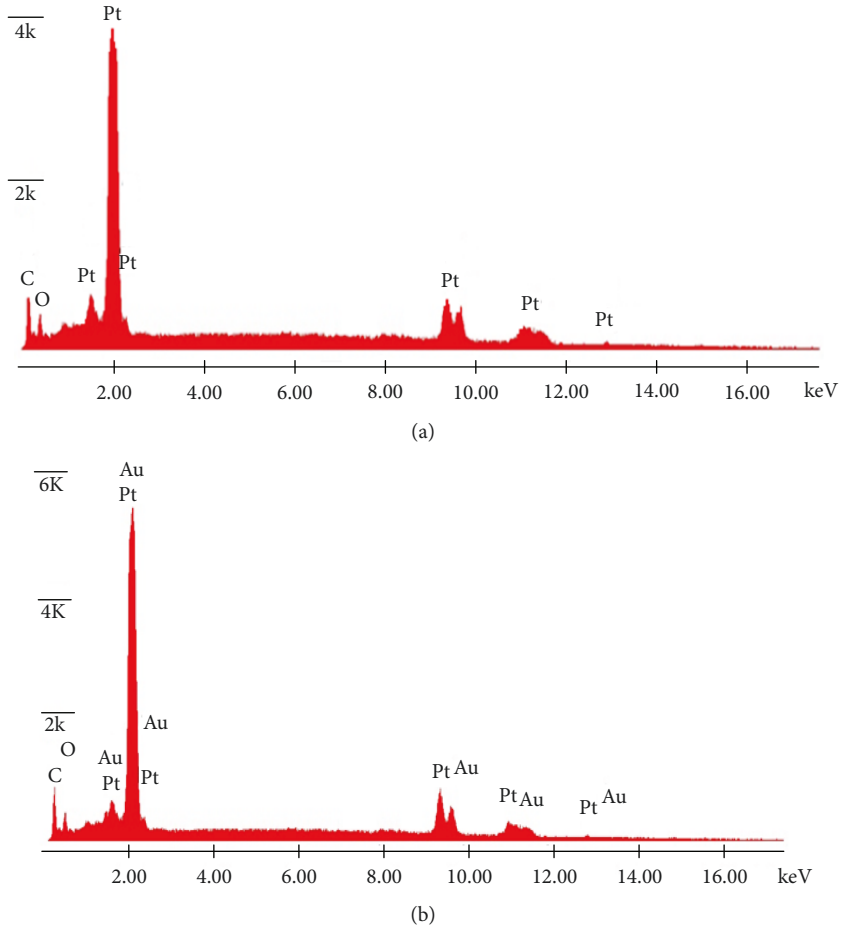

Figure 3: EDS analysis of (a) Pt/GC and (b) Au/Pt/GC electrodes.

electrode (Figure 5, a), the values of $I_p{}^d/I_p{}^{ind}$, $I_p{}^d/I_b$, and E_{onset} were ca. 0.92, 0.22, and −0.048 V, respectively. Though the inactiveness of AuNPs toward FAO [13], the Au/Pt/GC electrode (Figure 5, b), surprisingly, excelled the Pt/GC in the catalytic performance toward FAO with $I_p{}^d/I_p{}^{ind}$, $I_p{}^d/I_b$, and E_{onset} values of 3.44 (3.7 times higher), 0.54 (2.5 times higher), and −0.142 V (94 mV negative shift), respectively. This surely indicates the improved catalytic tolerance of the Au/Pt/GC electrode against CO poisoning that resulted from the facilitated FAO. Table 1 provides a summary of the electrochemical parameters obtained from Figure 5.

Additionally, as the criteria to prepare an efficient catalyst for commercialization purposes necessitates guarantying a

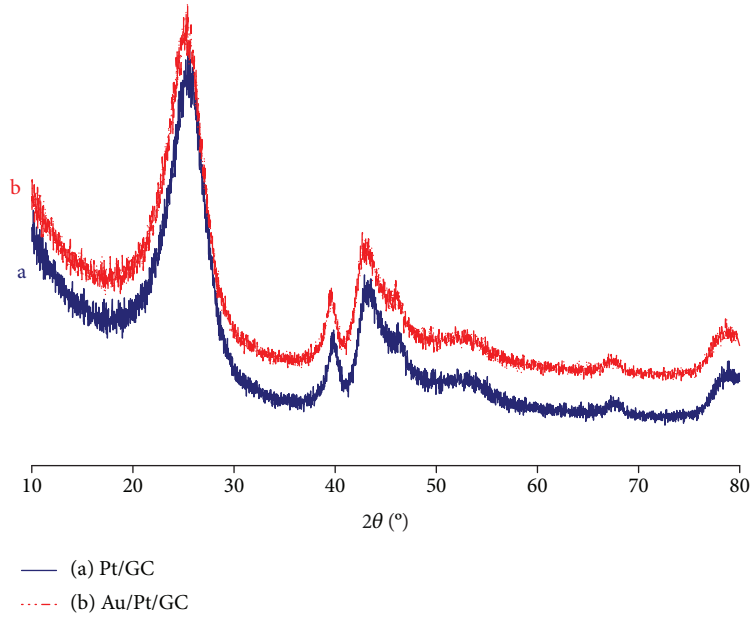

Figure 4: XRD analysis of (a) Pt/GC and (b) Au/Pt/GC electrodes.

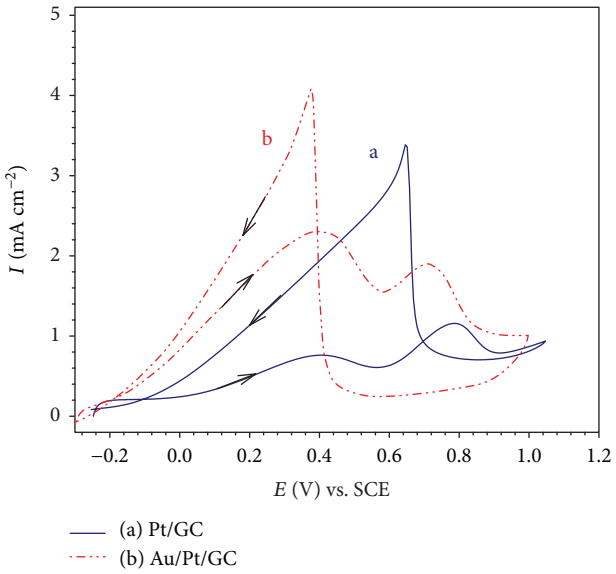

Figure 5: CVs obtained on (a) Pt/GC and (b) Au/Pt/GC electrodes in 0.1 M NaOH solution containing 0.3 M FA (pH = 3.5). Potential scan rate: 100 mV s^{-1}.

proper stability under continuous operations, the catalytic stability of the Au/Pt/GC catalyst was inspected. To evaluate this, CV measurements of FAO were carried out on the Pt/GC and Au/Pt/GC electrodes for 100 continuous cycles, and the corresponding $I_p{}^d$ values for all cycles were detected. Figure 6 confirmed once more the superiority of the Au/Pt/GC catalyst (Figure 6, b) where it exhibited after 100 CV cycles a higher (4.6 times) $I_p{}^d$ than that of the Pt/GC catalyst (Figure 6, a).

3.3. Electrocatalytic Activity and Stability toward MO. Figure 7 shows the CVs of the MO on the Pt/GC (Figure 7, a) and Au/Pt/GC (Figure 7, b) electrodes in 0.1 M NaOH solution containing 0.3 M FA. Generally, on Pt-based catalysts, the direct MO in alkaline solutions produces CO_2 according to the following equation [18, 19]:

$$CH_3OH + 6OH^- \longrightarrow CO_2 + 5H_2O + 6e^- \quad (8)$$

This reaction can be represented by the anodic peak observed at ca. 0.2 V in the forward scan of Figure 7, a, on the Pt/GC. During this process, the formation of poisonous intermediates such as CO is possible which mitigates the catalytic performance of MO (equation 9) [19].

$$CH_3OH + 3Pt \longrightarrow Pt - CO_{ads} + 2Pt + 4H^+ + 4e^- \quad (9)$$

Methane is another intermediate which can be produced during MO according to the following reaction [19, 20]:

$$Pt - CH_3 + Pt - H \longrightarrow Pt - CH_4 + 2Pt \quad (10)$$

It is worthy to mention here that the adsorbed –OH groups can further oxidize the poisonous CO and $-CH_3$ intermediates through the following reactions (equations 11 and 12, respectively);

$$Pt - CO_{ads} + -OH_{ads} \longrightarrow CO_2 + H^+ + e^- + Pt \quad (11)$$

$$Pt - CH_3 + 2(-OH_{ads}) \longrightarrow CO_2 + 5H^+ + 5e^- + Pt \quad (12)$$

Two functions can, therefore, be evaluated to assess the degree of catalytic enhancement toward MO. The first is the $I_p{}^d/I_b$ ratio that indicates the degree of resistance of

Table 1: Electrochemical parameters, extracted from Figures 4, 6, and 8 of the Pt/GC and Au/Pt/GC electrodes.

Electrode	FAO			MO		EGO	
	I_p^d/I_p^{ind}	I_p^d/I_p^b	E_{onset} (mV)	I_p^d/I_p^b	E_p^d (mV)	I_p^d (mA cm^{-2})	E_{onset} (mV)
Pt/GC	0.92	0.22	−0.048	3.81	0.23	1.62	−0.486
Au/Pt/GC	3.44	0.54	−0.142	5.45	0.01	5.61	−0.640

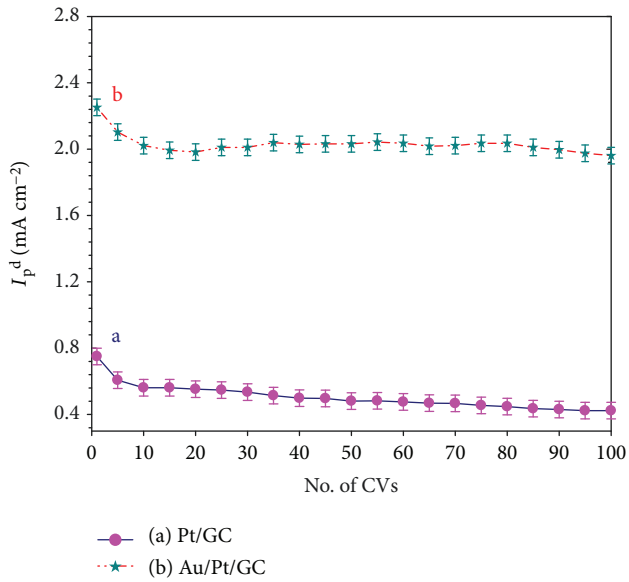

Figure 6: Stability measurement (I_p^d vs. no. of CVs) for FAO on (a) Pt/GC and (b) Au/Pt/GC electrodes. CVs were measured as in Figure 5.

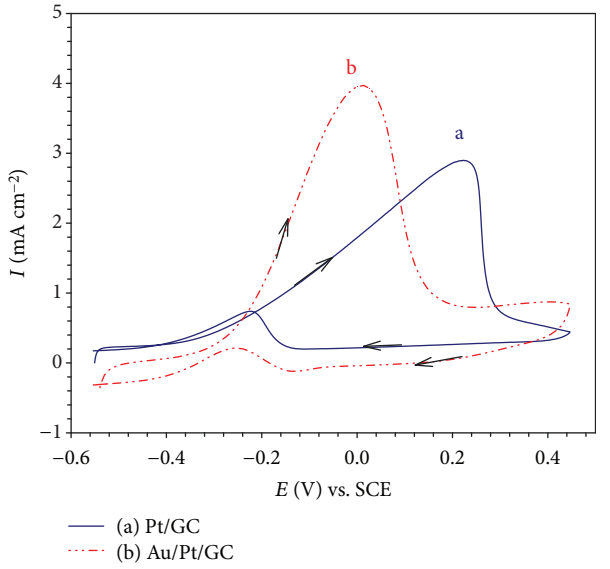

Figure 7: CVs obtained on (a) Pt/GC and (b) Au/Pt/GC electrodes in 0.1 M NaOH solution containing 0.3 M methanol. Potential scan rate: 100 mV s^{-1}.

the electrode to poisoning. The higher the ratio the catalyst may exhibit, the higher the catalytic performance and the higher the catalytic tolerance against poisoning the catalyst will have. The second is the peak potential of MO (E_p^d) that infers thermodynamically about power saving. At the Pt/GC electrode (Figure 7, a), the values of I_p^d/I_b and E_p^d were ca. 3.81 and 0.23 V, respectively. Taking into consideration the inactiveness of AuNPs toward MO in the recorded potential domain [21], the Au/Pt/GC electrode (Figure 7, b) was more active than the Pt/GC catalyst toward MO with I_p^d/I_b and E_p^d values of 5.45 (1.4 times higher) and 0.01 V (220 mV negative shift), respectively. That also indicates the improved catalytic tolerance of the Au/Pt/GC electrode against poisoning that ultimately resulted in enhanced MO. Table 1 summarizes the electrochemical parameters obtained from Figure 7.

To test the durability of the Au/Pt/GC electrode toward MO, continuous CV measurements of MO were carried out at the Pt/GC and Au/Pt/GC electrodes for 100 cycles. The corresponding I_p^d values for all cycles (Figure 8) confirmed the higher activity (twofold) and stability of the Au/Pt/GC catalyst.

3.4. Electrocatalytic Activity and Stability toward EGO. The electrocatalytic EGO in alkaline medium is a complex reaction because the presence of several adsorbed intermediates and reaction products/by-products can easily poison the catalysts [22]. Theoretically, EGO reaction proceeds with the formation of CO_2 according to the following equation [22]:

$$HOCH_2 - CH_2OH + 10OH^- \longrightarrow 2CO_2 + 8H_2O + 10e^- \quad (13)$$

However, in reality, the main product of EGO is oxalate which results from the partial oxidation of EG. Equation 14 and the two peaks observed at ca. −0.05 and 0.2 V in the forward scan of Figure 9, a, at the Pt/GC represent this pathway.

$$HOCH_2 - CH_2OH + 10OH^- \longrightarrow (COO^-)_2 + 8H_2O + 8e^- \quad (14)$$

Matsuoka et al. suggested that there are two pathway (poisoning and nonpoisoning) mechanisms for EGO on the Pt surface in alkaline media [23]. According to this mechanism, EG can be oxidized to oxalate via a non-poisoning pathway or to formate via a poisoning pathway. The poisoning pathway means further the oxidation of formate to poisoning CO species [22] (see Equation 5). Again, in alkaline medium, the adsorbed –OH groups can further speed the oxidation of poisonous CO to CO_2 according to Equation 11.

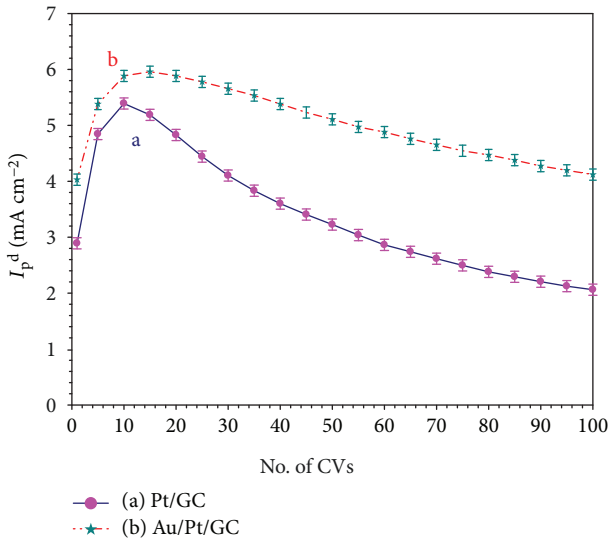

FIGURE 8: Stability measurement (I_p^d vs. no. of CVs) for MO on (a) Pt/GC and (b) Au/Pt/GC electrodes. CVs were measured as in Figure 7.

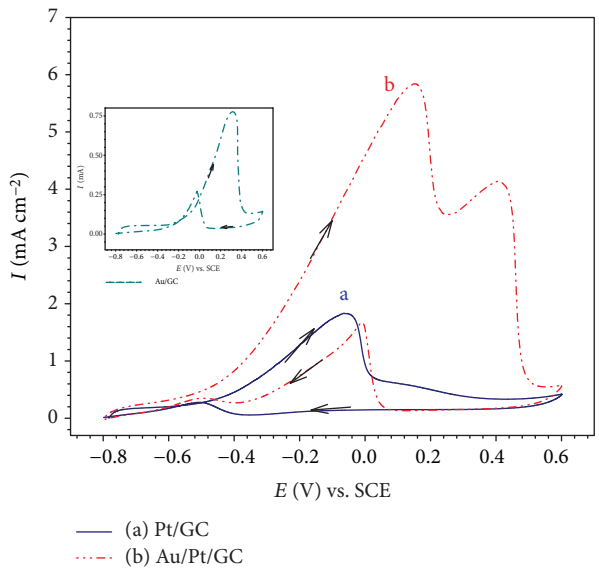

FIGURE 9: CVs obtained on (a) Pt/GC and (b) Au/Pt/GC electrodes in 0.1 M NaOH solution containing 0.3 M EG. Potential scan rate: 100 mV s^{-1}. Inset shows CV obtained on the Au/GC electrode in 0.1 M NaOH solution containing 0.3 M EG.

Herein, two functions will be employed to assess the degree of catalytic enhancement toward EGO. The first (I_p^d) indicates the degree of the direct (favorable) EGO, and the second is the E_{onset} of EGO. At the Pt/GC electrode (Figure 9, a), the values of I_p^d and E_{onset} were ca. 1.62 and −0.486 V, respectively. Interestingly, these values at the Au/Pt/GC electrode (Figure 9, b) jumped to 5.61 (3.5 times higher) and −0.640 V (154 mV negative shift), respectively, indicating improved kinetics and thermodynamics of EGO

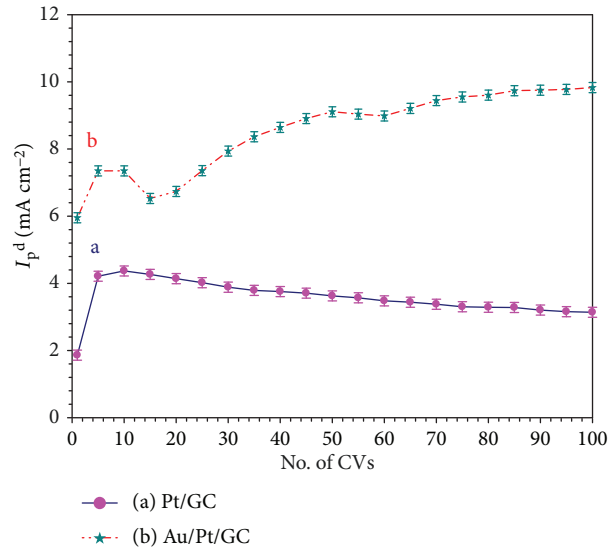

FIGURE 10: Stability measurement (I_p^d vs. no. of CVs) for EGO on (a) Pt/GC and (b) Au/Pt/GC electrodes. CVs were measured as in Figure 9.

at the Au/Pt/GC electrode. Table 1 also summarizes the electrochemical parameters obtained from Figure 9.

Finally, to inspect the catalyst stability during EGO, CV measurements of EGO were carried out at the Pt/GC and Au/Pt/GC electrodes for continuous 100 cycles. The corresponding I_p^d values for all cycles are depicted in Figure 10 to confirm the higher activity (3.1 times) and stability of the Au/Pt/GC catalyst.

3.5. Origin of Catalytic Enhancement. Generally, there are three different methodologies employed to increase the catalytic efficiency of the electrooxidation of liquid fuels on Pt-based materials [17]. One of these is recognized as the "ensemble or third-body effect" and is involved in surface modification or alloying of Pt particles with foreign atoms that minimize/prevent the adsorption of poisonous species. Interestingly, the modification we have made in this investigation for PtNPs with AuNPs proceeded in this line. In fact, the CO adsorption on Pt surfaces requires the existence of three neighboring Pt active sites with a certain geometry [24, 25]. Interruption of this continuity by AuNPs could accomplish this distortion to hinder the CO surface poisoning [25].

Interestingly, the catalytic performance of the Au/Pt/GC catalyst that we developed excelled the performance of other catalysts (see for example the Pt-Pd catalyst [26, 27]) toward the oxidation of FAO, MO and EGO. Table 2 provides a quick comparison between the two systems.

4. Conclusion

A simple modification for the conventional Pt/GC catalyst (typical anodic catalyst in liquid fuel cells) with gold nanoparticles (AuNPs) was intended for enhanced formic acid, methanol, and ethylene glycol electrooxidation (FAO, MO,

Table 2: A comparison of the obtained electrochemical parameters from this study (Pt-Au catalyst) and others obtained previously from the literature (Pt-Pd catalyst) for the oxidation of the three investigated fuels (FAO, MO, and EGO).

Catalyst	FAO I_p^d/I_p^{ind}	MO I_p^d/I_p^b	EGO Enhancement factor	Reference
Pt-Pd	0.87	1.23	3.3	[26, 27]
Pt-Au	3.44	5.45	3.5	This study

and EGO, respectively). The surface modification of Pt nanoparticles (PtNPs) with AuNPs could successfully interrupt their contiguity to resist the critical CO poisoning which stands as a major defect of their corresponding liquid fuel cells (DFAFCs, DMFCs, and DEGFCs, respectively). Interestingly, the modification with its inspired decorated structure at the Au/Pt/GC electrode could enhance the catalytic performance of FAO, MO, and EGO (as inferred from steering the mechanism toward the favorable (less energetic) pathway and lowering concurrently the onset potential). This enhancement appeared principally by mitigating the CO adsorption at the Pt surface which was blocking the Pt surface from the favorable oxidation pathway.

Data Availability

The data used to support the findings of this study are available from the corresponding author upon request.

Conflicts of Interest

The authors declare that there is no conflict of interest regarding the publication of this paper.

Acknowledgments

This research was supported by the British University in Egypt under the Young Investigator Research Grant (YIRG2017-03) and by the General Scientific Research Department at Cairo University (Grant 77/2016).

References

[1] "United States Environmental Protection Agency proposes affordable clean energy rule," https://www.epa.gov/laws-regulations.

[2] E. A. Olivetti and J. M. Cullen, "Toward a sustainable materials system," *Science*, vol. 360, no. 6396, pp. 1396–1398, 2018.

[3] J. A. Turner, "Sustainable hydrogen production," *Science*, vol. 305, no. 5686, pp. 972–974, 2004.

[4] I. M. Sadiek, A. M. Mohammad, M. E. El-Shakre, M. S. El-Deab, and B. E. El-Anadouli, "Enhanced electrolytic generation of oxygen gas at binary nickel oxide-cobalt oxide nanoparticle-modified electrodes," *Journal of Solid State Electrochemistry*, vol. 17, no. 3, pp. 871–879, 2013.

[5] S. Curtin and J. Gangi, "Fuel cell technologies market report 2014," in *DOE: Energy Efficiency and Renwable Energy*, US Department of Energy, 2014.

[6] D. Papageorgopoulos, *An Introduction to the 2010 Fuel Cell Pre-Solicitation Workshop*, US Department of Energy: Energy Efficiency and Renewable Energy, Lakewood, Colorado, 2010.

[7] I. M. Al-Akraa, A. M. Mohammad, M. S. El-Deab, and B. E. El-Anadouli, "Electrocatalysis by nanoparticle: enhanced electro-oxidation of formic acid at NiOx-Pd binary nanocatalysts," *Journal of the Electrochemical Society*, vol. 162, no. 10, pp. F1114–F1118, 2015.

[8] A. M. Mohammad, G. H. El-Nowihy, M. M. H. Khalil, and M. S. El-Deab, "Electrocatalytic oxidation of methanol at nanoparticle-based MnOx/NiOx/Pt ternary catalysts: optimization of loading level and order of deposition," *Journal of the Electrochemical Society*, vol. 161, no. 14, pp. F1340–F1347, 2014.

[9] G. H. El-Nowihy, A. M. Mohammad, M. M. H. Khalil, M. A. Sadek, and M. S. El-Deab, "Promising ethylene glycol electro-oxidation at tailor-designed NiOx/Pt nanocatalyst," *International Journal of Hydrogen Energy*, vol. 42, no. 8, pp. 5095–5104, 2017.

[10] N. M. Aslam, M. S. Masdar, S. K. Kamarudin, and W. R. W. Daud, "Overview on direct formic acid fuel cells (DFAFCs) as an energy sources," *APCBEE Procedia*, vol. 3, pp. 33–39, 2012.

[11] X. Yu and P. G. Pickup, "Recent advances in direct formic acid fuel cells (DFAFC)," *Journal of Power Sources*, vol. 182, no. 1, pp. 124–132, 2008.

[12] V. K. Gupta, M. L. Yola, N. Atar, Z. Üstündağ, and A. O. Solak, "Electrochemical studies on graphene oxide-supported metallic and bimetallic nanoparticles for fuel cell applications," *Journal of Molecular Liquids*, vol. 191, pp. 172–176, 2014.

[13] A. M. Mohammad, I. M. Al-Akraa, and M. S. El-Deab, "Superior electrocatalysis of formic acid electro-oxidation on a platinum, gold and manganese oxide nanoparticle-based ternary catalyst," *International Journal of Hydrogen Energy*, vol. 43, no. 1, pp. 139–149, 2018.

[14] G. A. El-Nagar and A. M. Mohammad, "Enhanced electrocatalytic activity and stability of platinum, gold, and nickel oxide nanoparticles-based ternary catalyst for formic acid electro-oxidation," *International Journal of Hydrogen Energy*, vol. 39, no. 23, pp. 11955–11962, 2014.

[15] M. Sakthivel and J.-F. Drillet, "Redox-transmetalation of Pt/Au catalyst for oxygen reduction reaction," *Electrochimica Acta*, vol. 120, pp. 73–79, 2014.

[16] F. Alardin, H. Wullens, S. Hermans, and M. Devillers, "Mechanistic and kinetic studies on glyoxal oxidation with Bi- and Pb-promoted Pd/C catalysts," *Journal of Molecular Catalysis A: Chemical*, vol. 225, no. 1, pp. 79–89, 2005.

[17] M. Shao, "Electrocatalysis in fuel cells," in *A Non- and Low-Platinum Approach*, Springer-Verlag, London, 2013.

[18] Z. D. Wei and S. H. Chan, "Electrochemical deposition of PtRu on an uncatalyzed carbon electrode for methanol electrooxidation," *Journal of Electroanalytical Chemistry*, vol. 569, no. 1, pp. 23–33, 2004.

[19] E. Urbańczyk, A. Jaroń, and W. Simka, "Ni Pt sinter as a promising electrode for methanol electrocatalytic oxidation," *International Journal of Hydrogen Energy*, vol. 43, no. 36, pp. 17156–17163, 2018.

[20] A. Jaroń and Z. Żurek, "Electrochemical properties of electrode obtained by cyclic oxidation and reduction of Ni powder," *ECS Transactions*, vol. 45, no. 21, pp. 89–95, 2013.

[21] Y.-Z. Su, M.-Z. Zhang, X.-B. Liu et al., "Development of Au promoted Pd/C electrocatalysts for methanol, ethanol and

isopropanol oxidation in alkaline medium," *International Journal of Electrochemical Science*, vol. 7, pp. 4158–4170, 2012.

[22] L. An and R. Chen, "Recent progress in alkaline direct ethylene glycol fuel cells for sustainable energy production," *Journal of Power Sources*, vol. 329, pp. 484–501, 2016.

[23] K. Matsuoka, Y. Iriyama, T. Abe, M. Matsuoka, and Z. Ogumi, "Electro-oxidation of methanol and ethylene glycol on platinum in alkaline solution: poisoning effects and product analysis," *Electrochimica Acta*, vol. 51, no. 6, pp. 1085–1090, 2005.

[24] A. Cuesta, M:. Escudero, B. Lanova, and H. Baltruschat, "Cyclic voltammetry, FTIRS, and DEMS study of the electrooxidation of carbon monoxide, formic acid, and methanol on cyanide-modified Pt(111) electrodes," *Langmuir*, vol. 25, no. 11, pp. 6500–6507, 2009.

[25] S. Zhang, Y. Shao, G. Yin, and Y. Lin, "Facile synthesis of PtAu alloy nanoparticles with high activity for formic acid oxidation," *Journal of Power Sources*, vol. 195, no. 4, pp. 1103–1106, 2010.

[26] M. S. Çögenli and A. B. Yurtcan, "Catalytic activity, stability and impedance behavior of PtRu/C, PtPd/C and PtSn/C bimetallic catalysts toward methanol and formic acid oxidation," *International Journal of Hydrogen Energy*, vol. 43, no. 23, pp. 10698–10709, 2018.

[27] D. N. Li, Y. M. He, J. J. Feng et al., "Facile synthesis of prickly platinum-palladium core-shell nanocrystals and their boosted electrocatalytic activity towards polyhydric alcohols oxidation and hydrogen evolution," *Journal of Colloid and Interface Science*, vol. 516, pp. 476–483, 2018.